

MODELLING THE RELEASE BEHAVIOUR OF CESIUM DURING SEVERE FUEL DEGRADATION

B.J. LEWIS,* B. ANDRE, B. MOREL AND P. DEHAUDT

*Commissariat à l'Energie Atomique, Centre d'Etudes Nucléaires de Grenoble,
Département de Thermohydraulique et de Physique, Service d'Etudes du Comportement du
Combustible, 17 rue des Martyrs, 38054 Grenoble Cedex 9, FRANCE*

D. MARO

*Commissariat à l'Energie Atomique, Centre d'Etudes Nucléaires de Fontenay aux Roses,
Institut de Protection et de Sécurité Nucléaire, Département de Protection de l'Environnement et des
Installations, Service d'Etudes sur les Accidents, BP6, 92265 Fontenay aux Roses, FRANCE*

M.F. OSBORNE AND R.A. LORENZ

*Oak Ridge National Laboratory, Chemical Technology Division, P.O. Box 2008, Oak Ridge,
Tennessee 37831-6221 U.S.A.*

ABSTRACT

An analytical model has been applied to describe the diffusional release of fission product cesium from Zircaloy-clad fuel under high-temperature reactor accident conditions. The present treatment accounts for the influence of the atmosphere (i.e., changing oxygen potential) on the state of fuel oxidation and the release kinetics. The effects of fuel dissolution on the volatile release behaviour (under reducing conditions) is considered in terms of earlier crucible experiments and a simple model based on bubble coalescence and transport in metal pools. The model has been used to interpret the cesium release kinetics observed in steam and hydrogen experiments at the Vertical Irradiation (VI) Facility in the Oak Ridge National Laboratory and at the HEVA/VERCORS Facility in the Commissariat à l'Energie Atomique.

1. INTRODUCTION

A temperature increase will result when there is insufficient cooling to remove the fission and decay heat from the nuclear fuel. During the progression of a reactor core melt, the temperature rise will escalate with the exothermic oxidation of the Zircaloy cladding material by steam.¹ The unoxidized Zircaloy cladding will also melt at a temperature dependent on its oxygen content, i.e., the melting point ranges from 2033 K (oxygen free) up to 2338 K (oxygen-saturated Zircaloy at ~35 at% oxygen). The molten cladding can liquefy the solid uranium dioxide fuel well below its melting temperature of 3100 K. Dissolution of the fuel in the molten Zircaloy will also cause a destruction of the matrix structure that may result in an enhanced release of volatile fission products. The hydrogen that is generated at high temperature by the steam oxidation of the core materials can influence the oxygen potential of the atmosphere. These high-temperature phenomena will directly influence the release characteristics of the fission products.² To better understand the mechanisms that govern the release behaviour under degraded fuel conditions, a number of single-effects annealing tests have been conducted at high-temperature in both oxidizing (steam) and reducing (hydrogen) conditions.^{3,4,5,6,7}

* *Visiting scientist from the Royal Military College of Canada, Department of Chemistry and Chemical Engineering, Kingston, Ontario, CANADA K7K 5L0.*

An analytical model has been developed to describe the diffusional release of cesium in terms of the state of fuel oxidation in annealing experiments (see Ref. 8). This treatment considers the inhibiting influence of hydrogen (produced by steam oxidation of the Zircaloy cladding) on the oxygen potential of the atmosphere, and its subsequent effect on the fuel oxidation kinetics. In this paper, the model is applied to the analysis of the vertical induction (VI) tests at the Oak Ridge National Laboratory (ORNL) and the HEVA/VERCORS tests at the Commissariat à l'Énergie Atomique (CEA). The amount of fuel dissolution that arises in the annealing tests with hydrogen is evaluated in terms of previous data from crucible experiments.^{9,10,11} The impact of liquefied fuel on the cesium release is assessed in terms of earlier theoretical work.^{12,13}

2. RESULTS AND ANALYSIS

2.1 Fission Product Release Model

As detailed in Ref. 8, fission-product transport in the uranium dioxide fuel matrix can be described by a diffusional release process. The generalized release fraction is given by:

$$F = F_D(\tau), \quad (1)$$

where the function $F_D(\tau)$ is given by the transformed Booth relation.^{6,14}

$$F_D = 6\sqrt{\frac{\tau}{\pi}} - 3\tau, \quad \text{for } \tau \leq 0.1, \quad (2)$$

$$F_D = 1 - \frac{6}{\pi^2} \exp\{-\pi^2 \tau\}, \quad \text{for } \tau > 0.1. \quad (3)$$

The dimensionless variable τ is evaluated from the integral relation

$$\tau = \int_0^t D'(t) dt = \sum_0^t D'(t) \Delta t, \quad (4)$$

where $D' = D/a^2$, D is a time-variable diffusion coefficient and a is the grain radius. The grain radius a is typically constant during the anneal since the grain boundaries are pinned by the fission product bubbles.¹⁵

The diffusion coefficient D (in m^2/s), as a function of temperature T (in K) and stoichiometry deviation x , can be given by the composite expression:⁸

$$D = D(T) + D(x, T). \quad (5)$$

Here the intrinsic diffusion component (as derived from isothermal experiments) is given by¹⁶

$$D(T) = 7.6 \times 10^{-10} \exp\left\{\frac{-7.0 \times 10^4}{RT}\right\}, \quad (6)$$

and the enhanced uranium vacancy production term is⁸

$$D(x,T) = D_o x^2 \exp\left\{\frac{-Q}{RT}\right\}, \quad (7)$$

where $R = 1.987$ cal/mol.K, $D_o = 2.22 \times 10^{-8}$ m²/s and $Q = 4.02 \times 10^4$ cal/mol. With oxidized fuel, one generally finds that $D(x,T) \gg D(T)$ in Eq. (5).

2.2 Fuel Oxidation Model

The process of fuel oxidation by steam is governed by a surface-exchange reaction at the solid/gas interface and not by the volume diffusion of oxygen into the solid.^{17,18,19,20} The kinetics of this reaction has been defined by

$$\frac{dx}{dt} = -\alpha (P_{H_2O})^m (S/V) [x - x_e], \quad (8)$$

where x_e is the equilibrium stoichiometry deviation (see Appendix A), α is the oxygen surface-exchange coefficient, m is the order of the reaction with respect to the steam pressure P_{H_2O} (in atm) and S/V is the surface-to-volume ratio of the solid.

The stoichiometry deviation x as a function of time can be calculated by integrating Eq. (8) over a given time step Δt of constant temperature T :

$$x(\Delta t) = x(0) \exp\{-\alpha (S/V) (P_{H_2O})^m \Delta t\} + x_e [1 - \exp\{-\alpha (S/V) (P_{H_2O})^m \Delta t\}], \quad (9)$$

where $x(0)$ is the value of the stoichiometry deviation at the beginning of the time step. The parameter α (m/s) has been determined experimentally by Cox et al. at 1 atm pressure in the temperature range 1073 to 1873 K (for sintered UO_2 with a geometric S/V).^{15,19}

$$\alpha = \alpha_o \exp\left\{-\frac{E}{RT}\right\} = 0.365 \exp\{-23500/T\}, \quad (10)$$

where T is in K. This parameter has also been evaluated by Abrefah et al. in the temperature range of 1273 to 1623 K, yielding similar coefficients of $\alpha_o = 0.450$ and $E/R = 22080$ K.²⁰

2.2.1 CEA Fuel Oxidation Experiments. To quantify the parameters of m and S/V in Eq. (8), further experiments were conducted using a thermogravimetry technique at the CEA. Sample pellets were cut into slices with a weight of 0.7 g and a diameter of 8 mm. These specimens were then placed into a Pt-mesh crucible in which a gaseous flow was introduced. The results from a typical experiment with

sintered UO_2 containing no open porosity are shown in Fig. 1. Equation (8) provides a good fit to the data using a calculated value of x_e based on the Lindemer and Besmann representation in Appendix A. Figure 2 shows a weight reduction resulting from fuel volatilization at 1773 K and 1873 K in an atmosphere of He-1% H_2O . A final reduction of the fuel sample in a hydrogen environment provides a measurement of the rate of UO_3 evaporation as shown in Fig. 3 as a function of temperature. Significant evaporation can be seen to occur above 1600 K.

Figure 4 shows the parameter $\alpha(P_{\text{H}_2\text{O}})^m$ as a function of temperature (considering evaporation effects) at a constant pressure of $P_{\text{H}_2\text{O}} = 0.01$ atm. This work yields an activation energy of $E/R = 23300$ K that is in good agreement with Eq. (10). The quantity $\alpha_o(P_{\text{H}_2\text{O}})^m$ can also be determined from Fig. 4. By repeating this experiment at various values of $P_{\text{H}_2\text{O}}$, the parameter m can be evaluated. Figure 5 suggests that the oxidation reaction rate depends on the square-root of the steam pressure in the low-pressure domain 0.01 to 1 atm, which is also in agreement with the findings of Abrefah et al.²⁰

Other experiments were conducted with samples of the same geometry but with an open porosity of 3%. Using a nitrogen adsorption technique, the specific surface area of these samples was measured to be $19 \text{ cm}^2/\text{g}$ compared to a geometric surface area of $0.5 \text{ cm}^2/\text{g}$, i.e., the $(S/V)_{\text{total}}$ is approximately 40 times the $(S/V)_{\text{geometric}}$. This open porosity consisted of a network of interconnected cracks ($\sim 10 \text{ }\mu\text{m}$ -thick) that were stable upon resintering at 1973 K in H_2 . As typically shown in Fig. 6, the oxidation rate is slightly higher for the fuel sample with 3% open porosity. From these results, an effective S/V is deduced from Eq. (8) such that $(S/V)_{\text{effective}} = 1.6$ to $2.3 (S/V)_{\text{geometric}}$. This finding is in good agreement with the earlier work for irradiated fuel.⁵ Thus, the effective surface area that arises in the oxidation reaction is much less than the specific area measured with the adsorption technique. This result occurs because of limited steam penetration into the microcracks. A relatively high partial pressure of hydrogen (produced from the fuel-oxidation reaction) in the microcracks may result in a low local value of x_e even though there is a large excess of H_2O in the bulk atmosphere.

2.3 ORNL Experiments

A series of anneals were conducted in the vertical induction (VI) facility at the ORNL.^{21,22,23,24,25,26,27} In these tests, fuel specimens were heated in either a hydrogen, steam or air environment at atmospheric pressure to temperatures ranging from 2000 to 2740 K. The fuel specimens consisted of 15-cm sections of high-burnup Light Water Reactor (LWR) fuel in which Zircaloy end caps were press fit on. A small 1.6-mm hole was drilled at the mid-length position to permit gas release during heating. The fission product release was monitored with on-line gamma ray spectrometry. A summary of the experimental conditions is given in Table 1. The measured release kinetics of the volatile cesium species and the temperature history are shown in Fig. 7 for the high-temperature VI tests 3 through 5.

2.3.1 Analysis of ORNL Experiments and Model Application. The ORNL Diffusion Model was obtained from a fitting of Eqs. (1) through (4) to the release data of the first five VI tests (irrespective of the atmospheric conditions).³ A simple regression was employed in this treatment to back-calculate the diffusion coefficient from the measured release fraction.^{28,29} Assuming a constant diffusivity over a short time period, an effective diffusion coefficient D (in m^2/s) was evaluated for the ORNL model as an Arrhenius function of temperature (T in K):^{3,28,29}

$$D = 7.63 \times 10^{-9} \exp\left\{-\frac{74300}{RT}\right\}, \quad (11)$$

If all of the input steam reaches the fuel-to-clad gap then $f_g = 1$. However, a previous Zircaloy-oxidation analysis for the VI-1 test indicated a significant bypass in the test section where only ~46% of the steam had actually reached the fuel specimen and reacted with the external-cladding surface.³³ Thus, if this fraction is then able to reach the gap, $f_g = 46\%$. Values of f_g for the other steam tests may be obtained from a suitable scaling of the VI-1 value by considering the ratio of the total quantity of hydrogen measured to that which occurs from complete Zircaloy oxidation. The total amount of molecular hydrogen produced from all sources in the steam tests is given by the area under the hydrogen rate curves (Fig. 8), yielding a value, for example, of 2.0 mol (VI-1) and 1.8 mol (VI-3); in comparison, the quantity of hydrogen produced from the Zircaloy/steam reaction can be calculated from the Zircaloy masses in Table 1 as 0.69 mol (VI-1) and 0.46 mol (VI-3). The result of this calculation yields an estimated value for f_g of 33% (VI-3) (see Fig. 7(a)).

The equilibrium stoichiometry deviation x_e can be estimated as a function of time for the ORNL steam tests. This calculation employs the fuel oxidation model of Eqs. (A-1), (A-4), (A-5) and (A-19), as well as the measured data for the steam input rates (R_{H_2O}) and hydrogen production rates (R_{H_2}) (Fig. 8), and bounding values of f_g . The stoichiometry deviation x can in turn be determined from Eqs. (9) and (10) where the S/V ratio is taken to be 490 m^{-1} . The value of x_e in Fig. 8 is observed to decrease under certain times when steam bypass becomes important. This decrease will therefore lead to a fuel reduction. In the present analysis, it is implicitly assumed that the reduction process occurs instantaneously, rather than by the slower kinetics of Eq. (9). This assumption is made because reduction is much more rapid than oxidation since the former process is solid-state diffusion controlled.²⁰ With a knowledge of $x(t)$, the cumulative release fraction can be estimated from the fission product release model of Eqs. (1) through (4). The combined diffusion coefficient of Eqs. (5), (6) and (7) is employed.

The result of the calculation for the VI-3 steam test is shown in Fig. 7(a) as labelled by the model $D(x, T)$ (with $f_g = 1$ and 0.33). In general, the release is underpredicted early in the test. This result occurs because release from grain-boundary cracking and from deposits on the internal clad surface have been ignored. On the other hand, the model tends to overpredict the release later in the experiment since the fuel oxidation is, in reality, more limited as a consequence of a reduced mass transport into the fuel-to-clad gap. The given release prediction is comparable to that of the empirical ORNL diffusion model. However, it is worthwhile to note that the present calculation is essentially a "blind" test since no adjustable factor is used.

A best-fit prediction can be provided for the VI-3 steam test by considering the second-order effects of release from the grain boundaries and fuel-to-clad gap. These effects can be incorporated into the combined fuel oxidation and fission product release model by replacing the intrinsic diffusivity of Eq. (6) with the effective diffusivity of Eq. (12). This change is only applied during the initial ramp below a temperature of 2000 K (VI-3) where $dT/dt > 0$. During this period, the hyperstoichiometric diffusivity is reduced since x is very small as a result of hydrogen production from the steam reaction with the Zircaloy cladding (see Fig. 8). Consequently, Eq. (12) will dominate for the ramp release. The reduced transport of steam to the fuel can be further modelled with an empirically-fit parameter f_g . In accordance with the earlier analysis, a best-fit value of $f_g = 26\%$ implies that only 80% of the steam, which actually reaches the reaction tube, enters into the fuel-to-clad gap through the drilled hole or cracks in the oxidized cladding. The release prediction is considerably improved, as indicated by the "best fit" model in Fig. 7(a).

In summary, the present analysis indicates that the atmospheric effects are less important in the ORNL tests as a consequence of a reduced oxygen potential in the steam tests (resulting from steam bypass and a reduced mass transport of steam to the fuel-to-clad gap).

where $R = 1.987 \text{ cal mol}^{-1} \text{ K}^{-1}$. This diffusion coefficient was recommended for the burnup range of 38 to 44 MWd/kg uranium. In most circumstances, Eq. (11) leads to an underprediction of the cumulative release fraction as labelled by the model "ORNL" in Fig. 7.

The VI tests 4 and 5 were conducted in a hydrogen environment at high temperature. Under these conditions, the diffusion component $D(x, T) = 0$ and intrinsic diffusion would be expected to predominate. As discussed in Ref. 6, the intrinsic diffusivity in Eq. (6) significantly underpredicts the release behaviour. However, a revised diffusion coefficient $D(T)$ (for hydrogen conditions) can be obtained from a specific fitting of the fission-product release model to the VI-4 and VI-5 data. Using a Marquardt-Levenberg algorithm for the regression analysis, the following diffusion coefficient (in m^2/s) is obtained:

$$D = 1.21 \times 10^{-7} \exp\left\{-\frac{79700}{RT}\right\}. \quad (12)$$

This diffusivity provides a much better release prediction for the hydrogen tests [labelled as $D(T)$ in Figs. 7(b) and 7(c)] than that proposed for the ORNL model in Eq. (11).

The fuel in the hydrogen experiments (VI-4 and VI-5) is expected to be close to stoichiometry for the following reasons. A "pure" hydrogen atmosphere will produce a low oxygen potential, where equilibrium thermodynamics predicts a hypostoichiometric phase for the urania.^{30,31} In fact, at higher temperature, a region exists where the UO_{2-x} is in equilibrium with liquid uranium (containing dissolved oxygen).³¹ However, this result was not observed in the ceramography of the hydrogen tests at the CEA (Section 2.4) or ORNL, which may indicate that the fuel was buffered somewhat by trace quantities of water vapour in the apparatus. Although the fuel can also be reduced on contact with the Zircaloy cladding, this reaction will be inhibited with the presence of an oxide layer on the inner surface of the cladding. This oxide layer will result from the liberation of oxygen with high fuel burnup. The fuel will also not increase in stoichiometry during the previous irradiation period as a consequence of this gettering of the oxygen by the cladding, as well as by the fission-product molybdenum.³² The poor wettability of the fuel after clad melt in the annealing experiments will also prevent significant fuel reduction (see Section 3). In conclusion, the present discussion suggests that the diffusivity in Eq. (12) should correspond to near-stoichiometric conditions.

A significant effect of the atmosphere on the release behaviour was not observed in the ORNL steam tests (VI-3). This result may be attributed to a lower oxygen potential resulting from steam bypass of the fuel test section and limited mass transport of steam into the fuel-to-clad gap of the fuel specimen.^{33,34} The bypassed steam also reacted with the graphite susceptor of the test assembly, liberating carbon monoxide and additional hydrogen. With limited fuel oxidation, the diffusivity in Eq. (12) should therefore apply. In fact, the use of this diffusivity in the model of Eqs. (1) through (4) also provides a good prediction of the release behaviour for the "steam" test (VI-3) (as labelled as $D(T)$ in Fig. 7(a)).

This analysis suggests that the oxygen potential is lower than expected in the various steam tests. This result can be further demonstrated with the use of the fuel oxidation and fission product release models (Sections 2.1 and 2.2). In this calculation, it is important to consider the mass transfer of steam to the fuel specimen and into the internal rod atmosphere. This effect can be quantified in terms of the parameter f_g in Eq. (A-19).

2.4 CEA Experiments

Eight annealing tests were performed in the HEVA facility at the Commissariat à l'Énergie Atomique (CEA)-Grenoble from 1983 to 1989 (see Table 2).^{7,35,36} In these tests, fuel specimens were heated in either a hydrogen or steam atmosphere between 1900 K to 2370 K. This program has been extended as the VERCORS test series in order to investigate the release behaviour of fission products in the presence of greater fuel deterioration at higher temperature. On-line gas chromatography was also used to monitor the hydrogen production for the tests after VERCORS-1.

Each test (except HEVA-7) was conducted with a small section of a spent Pressurized Water Reactor (PWR) fuel rod. The irradiated fuel specimen consisted of three pellets that were contained in the original Zircaloy-4 cladding. A half-pellet of depleted UO₂ was placed at each end of the fuel stack. The fuel was held in place by crimping the ends of the cladding (i.e., no end caps were used). In order to restore the short-lived inventory after the long cooldown periods, the fuel samples were reirradiated in the SILOE experimental reactor for ~6 days at 8 W/cm (HEVA tests) to 15 W/cm (VERCORS tests), after which the annealing tests were carried out within 50 h.

The measured release kinetics of the volatile cesium species are compared for the two high-temperature tests (HEVA-6 and VERCORS-2) in Fig. 9. An oxidative phase was performed in the early part of the HEVA-6 test, where the fuel specimen was exposed to a mixture of steam (25 mg/s) and hydrogen (0.2 mg/s) at a temperature of 1620 K for 50 min, in order to oxidize about two-thirds of the thickness of the Zircaloy cladding. The HEVA-6 test (see Fig. 9(a)) reached a maximum temperature plateau of 2370 K in a hydrogen atmosphere. A reducing environment is also expected to be present in the early phase of the test as a consequence of hydrogen production from the Zircaloy-steam reaction. In comparison, the VERCORS-2 test in Fig. 9(b) was carried out at 2150 K in a predominantly oxidizing (hydrogen/steam) environment. These experiments can provide a further validation of the models in Sections 2.1 and 2.2.

2.4.1 Model Application. Since the uranium dioxide fuel in the HEVA-6 test experienced a reducing environment, the fission product release model of Eqs. (1) to (4) can be directly applied with an intrinsic diffusion coefficient. As shown in Fig. 9(a), the diffusivity of Eq. (6) (derived from isothermal experiments) leads again to an underprediction of the ¹³⁷Cs release kinetics. On the other hand, it can be shown that the release kinetics are significantly overpredicted with the diffusivity of Eq. (12) (derived from the ORNL hydrogen tests). This difference may be related to the fact that cladding is present in an oxidized state throughout the HEVA-6 test (as a result of an initial oxidative phase), whereas the metallic cladding has melted and relocated in the ORNL hydrogen tests (VI-4 and VI-5). Thus, the enhanced release in the VI tests may be attributed to a lack of fuel constraint by the cladding or, perhaps, due to dissolution of the fuel by the molten Zircaloy (see Section 3).

A best fit diffusivity can be evaluated for the Heva-6 test using a Marquardt-Levenberg regression analysis (see Fig. 9(a)). This analysis indicates the presence of a shallow minimum where a number of fitting-parameter pairs (i.e., pre-exponential factor and activation energy) yield equivalent results. For instance, on fixing the activation energy to the value obtained for the VI-hydrogen experiments, the following optimized diffusivity (in m²/s) is obtained (compare with Eq. (12)):

$$D = 1.35 \times 10^{-8} \exp\left\{-\frac{79700}{RT}\right\}. \quad (13)$$

This diffusivity is approximately an order of magnitude smaller than that given in Eq. (12). The best-fit model is in good agreement with the observed release kinetics.

The fuel oxidation and cesium release model can be directly applied to the VERCORS-2 test (see Fig. 9(b)), which was conducted predominantly in a steam atmosphere. The oxygen potential for the given steam/hydrogen mixture can be evaluated with Eqs. (A-4), (A-5) and (A-19), where R_{H_2O} is the steam input rate and R_{H_2} is the sum of the hydrogen input rate and the measured hydrogen production rate (Fig. 10). The steam bypass can be similarly quantified by taking f_g in Eq. (A-19) as the ratio of the calculated amount of hydrogen produced from Zircaloy-clad oxidation to the total amount of hydrogen created (as measured by gas chromatography), i.e., $f_g = 370 \text{ mg H}_2 / 2126 \text{ mg H}_2 = 0.174$. The subsequent mass transport of steam to the gap was not limited in this case because the fuel specimen had no end caps. Hence, the equilibrium stoichiometry deviation (x_e) can be evaluated by equating the oxygen potential in the atmosphere to that of the solid using the Blackburn representation of Eq. (A-1). Following the methodology of Section 2.3.1, the stoichiometry deviation can, in turn, be calculated from Eqs. (9) and (10) for an S/V ratio of 490 m^{-1} . With the calculated $x(t)$ values in Fig. 10, the ^{134}Cs release kinetics can therefore be determined from the release model of Eqs. (1) through (4). The combined diffusivity of Eqs. (5), (6) and (7) is again used in this calculation. The grain radius is fixed as $a = 7.5 \text{ }\mu\text{m}$ (Table 2). As shown in Fig. 9(b), the model prediction is in good agreement with the measured data. To consider an enhanced release from the grain boundary and fuel-to-clad gap during the temperature ramp-up period (where $dT/dt > 0$) (see Section 2.3.1), the intrinsic diffusivity of Eq. (6) can be replaced by Eq. (13) (as deduced from the HEVA-6 test). However, there is essentially no change in the predicted release curve of Fig. 9(b) since the hyperstoichiometric term typically dominates the intrinsic one in Eq. (5) for the given experimental conditions.

In summary, comparing the CEA (Heva-6) and ORNL (VI-4 and VI-5) test results under hydrogen conditions, the loss of cladding support in the ORNL tests (as a result of melting and relocation) leads to an enhanced cesium release. The fuel oxidation and fission product release model, developed in Ref. 8, is able to reproduce the release kinetics in the Vercors-2 steam test (where again steam bypass effects must be considered).

3. DISSOLUTION PHENOMENA

In the ORNL steam tests (VI-1, VI-2 and VI-3), the fuel specimens had remained intact. However, fuel collapse was observed in the hydrogen tests (VI-4 and VI-5) above the melting temperature of the Zircaloy cladding. Radiation detectors along the axial length of the fuel column indicated that the fuel stack had collapsed at $\sim 2150 \text{ K}$ in VI-4 and between 2400 to 2700 K in VI-5.²⁵ It is believed that the cladding/fuel was in a semimolten state because of the degree of downward penetration of the fission products below the original fuel location.²⁴ Post-test metallography of the VI-4 assembly indicated a chemical interaction between the liquid Zircaloy-4 and the solid UO_2 . The effect of fuel dissolution on the release of the volatile fission products is considered in Section 3.1.

The oxygen content of the cladding must exceed a minimum value (e.g., $\sim 1 \text{ wt}\%$ at 2200 K) to provide sufficient wetting of the fuel for dissolution.^{9,10} Early in the VI-4 experiment, the wettability of the fuel was limited because the test was conducted in a reducing (hydrogen) atmosphere and the cladding was originally oxygen-free. Consequently, only weak $\text{UO}_2/\text{Zircaloy}$ chemical interaction is expected to occur after clad melt while the molten Zircaloy runs down the cracked fuel pellets; i.e., significant dissolution of the UO_2 can not occur until there is an increased oxygen content in the melt after fuel collapse into the molten pool.

The volume-percent of fuel dissolution expected in the VI-4 experiment can be estimated as follows. Recent crucible experiments have shown that the maximum solubility of UO_2 in liquid Zircaloy depends

on the $\text{UO}_2/\text{Zircaloy}$ mass ratio, the initial oxygen content of the cladding and the temperature of the melt. The time-dependent behaviour of the dissolution process can also be described by first-order kinetics:¹¹

$$C_U(t) = C_{U\infty}(1 - \exp(-k't)), \quad (14)$$

where $C_U(t)$ is the uranium concentration in solution at time t , $C_{U\infty}$ is the uranium concentration in the saturated melt, k' is the first-order rate constant $= k_U (S/V)_L$ (s^{-1}), k_U is the uranium assimilation rate constant (m/s), and $(S/V)_L$ is the fuel surface area/molten Zircaloy volume ratio (m^{-1}).

The crucible experiments in Ref. 11 were conducted with a $(S/V)_L$ ratio of 730 to 770 m^{-1} . In comparison, a lower-bound estimate of the $(S/V)_L$ for the VI-4 fuel specimen is $\sim 800 \text{ m}^{-1}$ using the fabricated geometry of the fuel specimen and neglecting any cracking effects for the irradiated pellets. Since the $(S/V)_L$ ratios are similar, Eq. (14) suggests that an equilibrium concentration should be reached at about the same time (or even more rapidly with a larger ratio) in the VI-4 experiment if convective stirring in the melt is not limited. For instance, the crucible experiments typically reached saturation in about 0.5 to 3 min within the temperature range of 2273 to 2473 K, where k' varied from 0.025 to 0.14 s^{-1} . On the other hand, the $\text{UO}_2/\text{Zircaloy}$ mass ratio was $m_{\text{UO}_2}/m_{\text{Zry}} \approx 11$ for the crucible experiments,¹¹ compared with a lower mass ratio of $m_{\text{UO}_2}/m_{\text{Zry}} = 78.2 \text{ g}/21.1 \text{ g} \approx 4$ for the VI-4 test (Table 1). A lower ratio for the VI-4 experiment will yield a greater amount of fuel dissolution at a given temperature, although this increase will be offset somewhat with a reduction of the ZrO_2 furnace tube by melt interaction; as the oxygen content of the melt increases, the amount of UO_2 that can be dissolved by the melt decreases.^{9,11}

In conclusion, the saturation concentration should be rapidly reached in the VI-4 test (with sufficient convective stirring) with a value comparable to that of the crucible experiments. The average temperature of the melt during the VI-4 test after fuel collapse was 2373 K. Hence, at this temperature it follows from the crucible experiments that $\sim 9\%$ of the volume of the fuel should dissolve when the Zircaloy is initially oxygen free.¹¹ This estimate can also be compared to that determined by a fission product release analysis for the VI-4 test (Section 3.1).

3.1 Fission Product Release With Fuel Dissolution

Based on mass balance considerations, the fractional release (F) of volatile fission products from the fuel with the occurrence of fuel dissolution is:

$$F = [F_D(\tau) - f\{F_D(\tau) - F_D(\tau_L)\}] + f[1 - F_D(\tau_L)]F_L(t), \quad (15)$$

where f is the volume fraction of fuel dissolution (see Section 3.), $F_D(\tau)$ is the release fraction for matrix diffusion [see Eqs. (2) and (3)], and $F_L(t)$ is the release fraction for dissolved fuel. It is assumed that fuel dissolution occurs at the dimensionless time $\tau = \tau_L$ (or time $t = t_L$). The first term in Eq. (15), i.e., $F_D(\tau) - f\{F_D(\tau) - F_D(\tau_L)\}$, corresponds to the diffusional component of release while the second term describes that from the dissolved fuel region. The release fraction for dissolved fuel is assumed to occur as a first-order rate process for time $t \geq t_L$,

$$F_L(t) = [1 - \exp(-k(t - t_L))], \quad (16)$$

where k is a rate constant of release. Since the process of fuel dissolution is rapid (see Section 3.), the dissolution kinetics can be modelled as a step function where t_L is the time of complete dissolution which is assumed to occur one minute after fuel relocation into the Zircaloy melt. Hence, for time, $t < t_L$, $f = 0$, and Eq. (15) simply reduces to the release fraction in Eq. (1); at time $t \geq t_L$, the parameter f is taken to be equal to the saturation value. By the time of fuel dissolution, a fraction $F_D(\tau_L)$ has already been released by diffusion from the fuel matrix.

The model in Eqs. (15) and (16) can be fit with a Marquardt-Levenberg algorithm to the VI-4 data in Fig. 7(b). For this calculation, the fraction $F_D(\tau_L)$ is fixed at 27% at ~58 min (based on the observed time of relocation). The additional fitting parameters of the generalized model are f and k . As shown in Fig. 7(b), better agreement is obtained when the effect of fuel dissolution is considered. The model parameters in this case are evaluated as $f = 3.7\%$ and $k = 4.6 \times 10^{-7} \text{ s}^{-1}$ (Table 3). A discussion of these results is presented in the following sections.

3.1.1 Volume Fraction of Fuel Dissolution (f). The fitted value of f (i.e., 3.7%) is comparable to that expected from the crucible experiments (i.e., 9%). The lower value for the VI-4 test may result from a higher oxygen content in the melt (from a reduction of the furnace tube by the melt) and, possibly, from limited convection in the melt (see Section 3.). The VI-4 result is also lower than that measured in a preliminary test (VT-4) with hollow and unirradiated pellets (~11%). This result is to be expected in light of the lower $\text{UO}_2/\text{Zircaloy}$ mass ratio in the VT-4 test.²⁴

3.1.2 Rate Constant for Volatile Release from Dissolved Fuel (k). The first-order rate constant k can be determined in terms of a physical process of bubble rise through a viscous melt. Considering a balance of forces for gravity and drag versus buoyancy, the terminal rise velocity $V_{b,t}$ (in m/s) for a submerged rigid bubble of radius r_b (in m) is given by,^{12,13}

$$V_{b,t} = \frac{2 r_b^2 \rho_L g}{9 \mu_L}, \quad (17)$$

where ρ_L is the density of the melt (kg/m^3), g is the gravitational constant ($= 9.807 \text{ m/s}^2$), and μ_L is the viscosity of the melt (Pa.s). To account for the tortuous path that the bubble must take in its upwardly-biased rise through the partially dissolved fuel pellets, the effective bubble rise velocity V_b is taken to be one-half of the terminal velocity.¹² Thus, the rate constant k for cesium release can be related to a time-averaged, bubble rise velocity $\langle V_b \rangle$ according to:

$$k = \frac{\eta \langle V_b \rangle}{\ell} = \zeta \langle r_b^2 \rangle, \quad (18)$$

where $\zeta = \eta \rho_L g / (9 \mu_L \ell)$, η is the molar ratio of cesium to total volatile gas in the fuel specimen, and ℓ is the characteristic thickness of the melt. The parameter η may be approximated for VI-4 by the mass ratio $m_{\text{Cs}} / (m_{\text{Cs}} + m_{\text{Xe}}) = 0.26 \text{ g} / (0.26 \text{ g} + 0.50 \text{ g}) = 34\%$.²⁴ From the metallographic examination, and a calculation of the total amount of cladding that is available for relocation, ℓ is estimated to be about 0.02 m. The physical parameters for the melt, ρ_L and μ_L , must also be obtained. Although the values for these and other parameters are given in Ref. 12 (for liquid UO_2), they are not referenced and, in several cases, have incorrect units. Consequently, an independent search was undertaken for the various quantities listed in Table 3.^{9,37,38,39,40,41} Hence, using Eq. (18) with the fitted value of k and the physical parameters in Table 3, the effective bubble radius is evaluated as $r_{b,\text{eff}} = [\langle r_b^2 \rangle]^{1/2} = 0.11 \text{ } \mu\text{m}$.

One can further estimate the amount of volatile gas present in bubbles compared to that which is trapped within porosity or dissolved in the liquefied fuel. This can be determined by accounting for bubble coalescence and growth in the liquefied medium. Using previous theoretical treatments,^{12,13,42,43} the effective bubble radius can be derived in Appendix B as given in Eq. (B-16). The only unknown quantity in Eqs. (B-16) and (B-17) is the available content of gas (M) that fixes the bubble density in Eq. (B-5). However, only a certain fraction (ϵ) of the total gas density in the melt (M_o) is available for bubble growth since some gas will remain dissolved in the molten pool or will be trapped in porosity, i.e., $M = \epsilon M_o$. The parameter M_o can be evaluated for the VI-4 test based on direct gamma spectrometry of the fuel specimen and an ORIGEN2 code calculation. Here the concentration of volatile gas is $C = 4.6 \times 10^{20}$ atom/cm³ of UO₂ (i.e., 7.3 kg of Xe/tU and 3.7 kg of Cs/tU).²⁴ Thus, the total gas atom density in the melt at the time of dissolution (τ_D) is

$$M_o = C(1 - F_D(\tau_D)) \left(\frac{V_{UO_2(L)}}{V_{UO_2(L)} + V_{Zr(L)}} \right), \quad (19)$$

where the volume of liquefied fuel is $V_{UO_2(L)} = f m_{UO_2} / \rho_{UO_2,m}$ and the volume of molten Zircaloy is $V_{Zr(L)} = m_{Zr} / \rho_{Zr,m}$. Using the data in Table 3, with $f = 3.7\%$ (Section 3.1.1), $F_D(\tau_D) = 27\%$, and the given masses for the fuel specimen in Table 1 (i.e., $m_{UO_2} = 78.2$ g and $m_{Zr} = 21.1$ g), M_o is evaluated as 2.8×10^{25} atom/m³. A value of $\epsilon = 13\%$ is finally obtained by equating Eq. (B-16) to the previous fitted value of $r_{b,eff} = \langle r_b^2 \rangle^{1/2} = 0.11$ μ m.

This analysis indicates that only ~13% of the fission gas is found in bubbles. The remaining gas is presumably in solution in the melt or located within the observed porosity (voids).

3.1.3 Discussion. The phenomenon of fuel dissolution, and its impact on the volatile release behaviour, are quantified in Sections 3.1.1 and 3.1.2. The present treatment explicitly assumes a single event for bubble nucleation in which the corresponding bubble growth is described by Eqs. (B-11) and (B-14). This formulation is supported by the fact that there is an in-situ supersaturation of fission gas during melt formation.

Liquefaction was only observed for those ORNL experiments performed in a reducing (hydrogen) atmosphere (VI-4 and VI-5). However, the dissolution process did not have a significant effect on the fission product release behaviour (see Fig. 7(b)). An instantaneous release is not indicated with fuel dissolution (as assumed in the NUREG-0772 fission product release correlation⁴⁴) because of limited growth of bubbles in the liquefied material. This finding is also supported in the analysis of Ref. 12. Only about 13% of the total cesium contained in the molten fuel is released via bubble transport (Section 3.1.2). The majority of the volatile cesium appears to remain in solution or is trapped inside voids. The low fraction of cesium in bubbles may reflect the presence of additional holdup mechanisms not considered explicitly in the model; for example, such phenomena may include: bubble nucleation in the pool, vapor diffusion of gas into bubbles, and the interaction/release of bubbles at the surface of the pool.⁴⁵ Caution should be exercised, however, in the use of the present results to real accident situations since it is not clear what impact the hydrogen carrier gas has on void production within the melt.

Inspection of the release curve in Fig. 7(c), suggests that only a diffusional release occurred from the fuel in the VI-5 experiment. Fuel relocation was observed much later in the VI-5 test (perhaps at a temperature as high as 2700 K) compared to that in VI-4 because of the lower burnup of the fuel specimen.²⁵ By the time of relocation in VI-5, most of the release would have already occurred by diffusion (i.e., $F_D(\tau_D) = 0.95$ in Eq. (15)).

Finally, in the CEA experiment performed in a reducing environment (HEVA-6), some Zircaloy penetration was observed in the fuel cracks. However, the fuel specimen remained intact as a consequence of the early steam period in which the cladding was partially oxidized (see Section 2.4), i.e., a protective (inner) zirconium oxide layer, produced early in the test (during the 1620 K temperature plateau), would prevent significant Zircaloy/ UO_2 interaction. Thus, the total amount of fuel dissolution is expected to be small, leading to a predominant diffusional release in Fig. 9(a).

4. CONCLUSION

1. An analytical model has been applied to describe the release behaviour of fission product cesium from uranium dioxide fuel during severe reactor accident conditions. In the present framework, the fission product release kinetics are based on the state of fuel oxidation, in accordance with a generalized diffusional approach. The fuel oxidation kinetics are detailed by a surface-exchange reaction at the fuel/steam interface. The effect of a changing oxygen potential in the atmosphere (due to the Zircaloy/steam reaction) is explicitly treated in the model.
2. The influence of pressure, fuel porosity and UO_3 volatilization on the fuel oxidation behaviour has been investigated in experiments at the CEA. The model has been applied to the ORNL (VI-3 through 5) and CEA (HEVA-6 and VERCORS-2) tests performed under various atmospheric and temperature conditions (i.e., in steam and hydrogen at 2150 to 2740 K).
3. A significant difference in the release was not observed between the hydrogen and "steam" tests at the ORNL and CEA since the oxygen potential was reduced as a result of hydrogen production from the Zircaloy/steam reaction. In addition, a significant steam bypass occurred at both facilities, resulting in additional hydrogen liberation from a steam reaction with the graphite susceptor of the furnace assembly. Limited transport of steam to the fuel-to-clad gap also reduced the fuel oxidation kinetics.
4. Intrinsic diffusivities were evaluated from release data in the hydrogen tests at the CEA (Heva-6) and ORNL (VI-4 and VI-5). These diffusivities were larger than those reported in earlier isothermal experiments, which may be related to temperature ramp effects. Fuel collapse was observed in the ORNL tests (VI-4 and VI-5) following clad melt and relocation; however, the clad remained intact in the Heva-6 test as a result of an earlier oxidative phase. The loss of cladding support yielded an increased diffusivity by an order of magnitude.
5. A small amount of fuel dissolution occurred in the ORNL hydrogen tests following clad melt. The fuel dissolution kinetics in the VI-4 test were analyzed in terms of separate-effects crucible experiments. The amount of volatile release from the dissolved fuel was assessed with a simple model based on the phenomena of bubble coalescence and buoyancy rise in a molten pool. The VI-4 analysis indicates that volatile release from dissolved fuel can be inhibited by bubble dynamics and porosity in the melt.

ACKNOWLEDGEMENTS

The CEA experiments were supported by the IPSN and Electricité de France. The ORNL experiments were sponsored by the U.S. Nuclear Regulatory Commission, Office of Nuclear Regulatory Research, Division of Systems Safety Research, Accident Evaluation Branch. The work at the RMC was supported by the Academic Research Program of the Department of National Defence of Canada (allocation no. 3705-882) and the Natural Sciences and Engineering Research Council of Canada (award no. OGP0155726).

APPENDIX A: CALCULATION OF x_e

The equilibrium deviation from stoichiometry (x_e) in Eq. (9) is determined by equating the equilibrium oxygen pressure in the solid (Section A.1) with that of the gas mixture (in the fuel-to-clad gap) (Section A.2).⁵

A.1 Oxygen Partial Pressure in the Solid

The partial pressure of oxygen p_{O_2} (in atm) of the solid, as a function of temperature (in K), is given by either the Blackburn thermochemical model:³⁰

$$\ln p_{O_2} = 2 \ln x - 2 \ln(1-x) + 2 \ln(2+x) + 108 x^2 - \frac{32700}{T} + 9.92, \quad (\text{A-1})$$

or the solid solution representation of Lindemer and Besmann:³¹

$$\ln p_{O_2} = \frac{-43298}{T} + 25.74 + 4 \ln \left[\frac{2x(1-2x)}{(1-4x)^2} \right], \quad \text{for } x \leq 0.01, \quad (\text{A-2})$$

$$\ln p_{O_2} = -\frac{37621}{T} + 15.15 + 2 \ln \left[\frac{x(1-2x)^2}{(1-3x)^3} \right], \quad \text{for } x > 0.01. \quad (\text{A-3})$$

A.2 Oxygen Partial Pressure in the Atmosphere

At a total system pressure p_t (in atm), the p_{O_2} in the gas mixture can be estimated from the transcendental equation:⁴⁶

$$K_1 (p_{O_2})^{1/2} \left[\left(\frac{Q_a}{2} - 1 \right) + \left(\frac{Q_a}{2} + 1 \right) \frac{p_{O_2}}{p_t} \right] = 1 - (Q_a + 1) \left(\frac{p_{O_2}}{p_t} \right), \quad (\text{A-4})$$

where $K_1 = \exp\{-\Delta G^0/RT\}$, $\Delta G^0 = -250800 + 57.8T$ J/mol and $R = 8.3145$ J/mol.K. The parameter Q_a is the hydrogen-to-oxygen atom ratio of the environment:⁵

$$Q_a = 2 \left(1 + \frac{n_{H_2}}{n_{H_2O}} \right), \quad (\text{A-5})$$

where n_{H_2}/n_{H_2O} is the ratio of the number of moles of hydrogen-to-steam in the gas mixture.

Alternatively, Eqs. (A-4) and (A-5) can be replaced by considering the equilibrium constant K_2 for water vapour decomposition for the reaction:



The parameter K_2 is given in several references. For example, from the definition of K_1 in Ref. 46, the equivalent expression for K_2 is:

$$\text{Olander: } \log K_2 = -\frac{26200}{T} + 6.032, \quad (\text{A-7})$$

where T is in K. Other representations for K_2 include, respectively:^{47,48,49}

$$\text{Wheeler and Jones: } \log K_2 = -\frac{25026}{T} + 1.958 \log T - 0.9659, \quad (\text{A-8})$$

$$\text{Nernst: } \log K_2 = -\frac{25300}{T} + 1.75 \log T - 1.2, \quad (\text{A-9})$$

$$\text{Ulich: } \log K_2 = -\frac{25300}{T} + 4.64 + 1.04(0.0007 T - 0.2). \quad (\text{A-10})$$

The oxygen partial pressure p_{O_2} can be evaluated at equilibrium at a given temperature T from the law of mass action for the given reaction in Eq. (A-6):

$$K_2 = \frac{p_{O_2} p_{H_2}^2}{p_{H_2O}^2}, \quad (\text{A-11})$$

and the laws of conservation of mass for H and O:

$$p_{H_2O} + p_{H_2} = (p_{H_2O})_i + (p_{H_2})_i, \quad (\text{A-12})$$

$$p_{H_2O} + 2p_{O_2} = (p_{H_2O})_i, \quad (\text{A-13})$$

where $(p_{H_2O})_i$ and $(p_{H_2})_i$ are the initial water and hydrogen partial pressures that are introduced into the gas mixture. Equations (A-11) through (A-13) lead to a cubic equation for the oxygen partial pressure, analogous to Eq. (A-4):

$$4(p_{O_2})^3 + 4[(p_{H_2})_i - K_2]p_{O_2}^2 + [(p_{H_2})_i^2 + 4(p_{H_2O})_i K_2]p_{O_2} - (p_{H_2O})_i^2 K_2 = 0. \quad (\text{A-14})$$

Two cases are of particular interest:

- (i) When only pure steam is introduced (i.e., there is no cladding present or the cladding is fully oxidized), the solution for the p_{O_2} is:

$$p_{O_2} = \left(\frac{K_2 p_{H_2O}^2}{4} \right)^{1/3}; \quad (\text{A-15})$$

- (ii) When a mixture of steam and hydrogen is introduced (i.e., the cladding is still oxidizing), such that there is a significant contribution of hydrogen, i.e., $K_2 \ll (p_{H_2})_i$, $4K_2 \ll (p_{H_2})_i^2 / (p_{H_2O})_i$, $4(p_{O_2})^3 \ll (p_{H_2O})_i^2 K_2$ and $4p_{O_2} \ll (p_{H_2})_i$, Eq. (A-14) reduces to:

$$p_{O_2} = \frac{(p_{H_2O})_i^2}{(p_{H_2})_i} K_2. \quad (\text{A-16})$$

Equations (A-8) and (A-16) yield the usual Wheeler and Jones formula for the oxygen potential in a hydrogen and steam mixture:⁴⁷

$$\ln p_{O_2} = -\frac{57625}{T} + 4.509 \log T - 2.224 - 4.605 \log \left(\frac{n_{H_2}}{n_{H_2O}} \right). \quad (\text{A-17})$$

As expected, if $n_{H_2} \ll n_{H_2O}$, Eq. (A-5) reduces to the pure steam condition, $Q_a = 2$. In this situation, Eq. (A-4) simplifies to an explicit expression for the p_{O_2} .⁴⁶

$$p_{O_2} = \left(\frac{p_i^2}{4K_1^2} \right)^{1/3}. \quad (\text{A-18})$$

which yields the same result as Eq. (A-15).

The molar ratio n_{H_2}/n_{H_2O} in Eqs. (A-5) or (A-17) can be estimated from the bulk-stream conditions at the mid-point of the fuel specimen using the measured hydrogen production rate R_{H_2} (in mol/s) and the steam input rate into the reaction tube R_{H_2O} (mol/s):

$$\frac{n_{H_2}}{n_{H_2O}} = \frac{\frac{1}{2} R_{H_2}}{f_g R_{H_2O} - \frac{1}{2} R_{H_2}}. \quad (\text{A-19})$$

Here f_g is the fraction of steam that enters into the fuel-to-clad gap from the mass transfer.

APPENDIX B: BUBBLE COALESCENCE AND GROWTH IN LIQUEFIED MEDIUM

Considering a single bubble-class size, the rate of change of the bubble density N_b (bubble/m³) moving by both random and biased motion in the liquefied medium is^{12,13}

$$\frac{dN_b}{dt} = -(16\pi r_b D_b + 4\pi r_b^2 V_b) N_b^2, \quad (\text{B-1})$$

where D_b is the bubble diffusivity. The first term in Eq. (B-1) accounts for random motion due to bubble diffusion (the full derivation of this term is given in Ref. 41). The second term describes the bias motion and corresponds to the product of the bubble density and the interaction volume swept out by each

bubble.^{12,13} The bubble velocity V_b (derived from Eq. (17)) is appropriate since the temperature distribution across the bottom section of the fuel assembly was uniform in the VI-4 test. However, if a temperature gradient were present, bubble transport may also occur by a volume diffusion or vapour transport mechanism, in addition to that of buoyancy (see Ref. 12).

The fission gas bubbles will migrate with a bubble diffusivity given by:¹²

$$D_b = \frac{3\Omega}{4\pi r_b^3} D_U \quad (\text{B-2})$$

Here Ω is the atomic volume ($= 41 \times 10^{-30} \text{ m}^3$ per U atom) and D_U is the uranium-atom diffusivity. Equation (B-2) actually follows from arguments for volume diffusion of bubbles in UO_2 in the solid state.^{12,41} The effects of diffusion in a molten liquid is accounted for in the estimate of D_U . If there is no tendency for the melt to slip at the surface of the diffusing uranium atom, D_U (in m^2/s) is determined by the classical Stokes-Einstein equation^{42,43}

$$D_U = \frac{k_B T}{6\pi r_U \mu_L} \quad (\text{B-3})$$

where k_B is Boltzmann's constant ($= 1.381 \times 10^{-23} \text{ J/K}$) and T is the temperature ($= 2373 \text{ K}$ for VI-4). The radius of the uranium particle r_U can be estimated from the atomic volume where $4\pi r_U^3/3 = \Omega$, which yields a value of $r_U = 2.1 \times 10^{-10} \text{ m}$.

Substituting the diffusivity (Eqs. (B-2) and (B-3)) and the bubble rise velocity V_b (Section 3.1.2) into Eq. (B-1), yields:

$$\frac{dN_b}{dt} = - \left[\frac{2\Omega k_B T}{\pi r_U \mu_L} \left(\frac{1}{r_b} \right)^2 + \frac{4\pi \rho_L g}{9\mu_L} (r_b)^4 \right] N_b^2 \quad (\text{B-4})$$

The relative importance of the two terms on the right side of Eq. (B-1) or (B-4) can be deduced by plotting the volume rate constants of $(dN_b/dt)/N_b^2$ as a function of the bubble radius (at the given temperature of 2373 K for the VI-4 experiment), i.e., the random motion will dominate for small bubbles less than $\sim 0.057 \mu\text{m}$, whereas bias motion will become important for larger bubbles. Consequently, the two phenomena in Eq. (B-4) can be decoupled.

For the VI-4 experiment, the amount of gas release from the melt is small since $kT_L \ll 1$, where $T_L \approx 29 \text{ min}$ ($= 1.74 \times 10^3 \text{ s}$) is the given period of release after dissolution. Thus, it can be assumed that the available quantity of gas M (in atom/m^3) in the melt is fixed such that

$$M = mN_b = \text{constant} \quad (\text{B-5})$$

The parameter m in Eq. (B-5) is the number of gas atoms contained in a bubble of radius r_b . This quantity can be evaluated from the equation of state for the gas atoms in the bubbles, and from a mechanical force balance for an equilibrium bubble in the liquid medium, i.e.,⁴¹

$$m = \frac{4\pi r_b^3/3}{B + (k_B T/2\gamma_L)r_b}, \quad (\text{B-6})$$

where B is the Van der Waals parameter ($= 85 \text{ \AA}^3/\text{atom}$ for xenon) and γ_L is the surface tension of the liquid medium. For the given value of γ_L and temperature (Table 3), bubble coalescence will be sufficiently rapid so that $B \ll (k_B T/2\gamma_L)r_b$, and Eq. (B-6) will therefore reduce to

$$m = \left(\frac{4\pi r_b^2}{3}\right) \left(\frac{2\gamma_L}{k_B T}\right). \quad (\text{B-7})$$

Thus, combining Eqs. (B-5) and (B-7), one obtains a relation between the bubble radius and bubble density:

$$\left(\frac{1}{r_b}\right)^2 = \left(\frac{8\pi\gamma_L}{3Mk_B T}\right) N_b. \quad (\text{B-8})$$

Considering only random motion for the moment, on substituting Eq. (B-8) into (B-4), yields

$$\frac{dN_b}{dt} = -\left(\frac{16\Omega\gamma_L}{3r_U\mu_L M}\right) N_b^3. \quad (\text{B-9})$$

Integrating this equation, and applying the initial condition $N_b(t=0) = N_{bo}$, gives

$$\frac{1}{N_b^2} = \frac{1}{N_{bo}^2} + \left(\frac{32\Omega\gamma_L}{3r_U\mu_L M}\right) t. \quad (\text{B-10})$$

After several generations of coalescence, the condition $N_b \ll N_{bo}$ applies, and the first term on the right hand side of Eq. (B-10) can be neglected.⁴¹ Finally, expressing this resultant equation in terms of the bubble radius with the use of Eq. (B-8) yields

$$r_{b,random}^2(t) = \left(\frac{k_B T}{\pi}\right) \left[\frac{3M\Omega}{2\gamma_L r_U \mu_L}\right]^{1/2} t^{1/2}. \quad (\text{B-11})$$

This equation is only valid while random motion dominates, i.e., from time $0 \leq t \leq t_o$. The time t_o is evaluated from Eq. (B-11) in which $r_{b,random}(t_o) = r_{bo} = 0.057 \text{ \mu m}$.

Similarly, when the bias motion predominates, Eqs. (B-4) and (B-8) lead to the differential equation:

$$\frac{dN_b}{dt} = -\left[\frac{\rho_L g}{16\pi\mu_L} \left(\frac{Mk_B T}{\gamma_L}\right)^2\right], \quad (\text{B-12})$$

or equivalently,

$$\left(\frac{1}{r_b^3}\right) \frac{dr_b}{dt} = \left[\frac{\rho_L g M k_B T}{12 \mu_L \gamma_L}\right] \quad (\text{B-13})$$

Separating variables in Eq. (B-13), and integrating from time t_o to t (where $r_b(t_o) = r_{bo}$), yields the result

$$r_{b,bias}^2 = \left\{ \frac{1}{r_{bo}^2} - \left[\frac{\rho_L g M k_B T}{6 \mu_L \gamma_L} \right] (t - t_o) \right\}^{-1} \quad (\text{B-14})$$

In light of Eq. (18), $\langle r_b^2 \rangle$ can be evaluated as

$$\langle r_b^2 \rangle = \int_0^{T_L} r_b^2(t) dt / \int_0^{T_L} dt = \frac{1}{T_L} \left\{ \int_0^{t_o} r_{b,random}^2 dt + \int_{t_o}^{T_L} r_{b,bias}^2 dt \right\}, \quad (\text{B-15})$$

where time zero starts from the time of dissolution. Substituting Eqs. (B-11) and (B-14) into Eq. (B-15), and performing the integration, gives the final result

$$\langle r_b^2 \rangle = \frac{1}{T_L} \left[\frac{2}{3} \phi_1 t_o^{3/2} - \frac{1}{\phi_2} \ln \{ 1 - r_{bo}^2 \phi_2 (T_L - t_o) \} \right], \quad (\text{B-16})$$

where

$$\phi_1 = \left(\frac{k_B T}{\pi} \right) \left[\frac{3 M \Omega}{2 \gamma_L r_U \mu_L} \right]^{1/2}, \quad \phi_2 = \frac{\rho_L g M k_B T}{6 \mu_L \gamma_L} \quad (\text{B-17})$$

REFERENCES

1. R.R. Hobbins, D.A. Petti, J. Osetek and D.L. Hagrman, "Review of Experimental Results on Light Water Reactor Core Melt Progression," Nucl. Technol. 95 (1991) 287.
2. R.R. Hobbins, D.A. Petti and D.L. Hagrman, "Fission Product Release From Fuel Under Severe Accident Conditions," Nucl. Technol. 101 (1993) 270.
3. M.F. Osborne and R.A. Lorenz, "ORNL Studies of Fission Product Release Under LWR Severe Accident Conditions," Nucl. Safety 33 (1992) 344.
4. B.J. Lewis, F.C. Iglesias, C.E.L. Hunt and D.S. Cox, "Release Kinetics of Volatile Fission Products Under Severe Accident Conditions," Nucl. Technol. 99 (1992) 330.
5. B.J. Lewis, D.S. Cox and F.C. Iglesias, "A Kinetic Model for Fission-Product Release and Fuel Oxidation Behaviour for Zircaloy-Clad Fuel Elements Under Reactor Accident

- Conditions," *J. Nucl. Mater.* 207 (1993) 228.
6. A.C. Harnden-Gillis, B.J. Lewis, W.S. Andrews, P.L. Purdy, M.F. Osborne and R.A. Lorenz, "Modeling of Cesium Release from Light Water Reactor Fuel Under Severe Accident Conditions," *Nucl. Technol.* 109 (1995) 39.
 7. J.P. Leveque, B. Andre, G. Ducros, G. Le Marois and G. Lhiaubet, "The HEVA Experimental Program," *Nucl. Technol.* 108 (1994) 33.
 8. P.L. Purdy, B.J. Lewis, W.S. Andrews, D.S. Cox and F.C. Iglesias, "A Model for Fuel Oxidation and Diffusion-Based Fission Product Release Under Severe Nuclear Reactor Accident Conditions," 4th International Conference on CANDU Fuel, Pembroke, Canada, October 1-4, 1995.
 9. P. Hofmann, D. Kerwin-Peck and P. Nikolopoulos, "Physical and Chemical Phenomena Associated with the Dissolution of Solid UO_2 by Molten Zircaloy-4," *Zirconium in the Nuclear Industry: Sixth International Symposium*, ASTM STP 824, D.G. Franklin and R.B. Adamson, Eds., American Society for Testing and Materials, 1984, p. 810-834.
 10. W. Dienst, P. Hofmann and D.K. Kerwin-Peck, "Chemical Interactions Between UO_2 and Zircaloy-4 from 1000 to 2000°C," *Nucl. Technol.* 65 (1984) 109.
 11. P.J. Hayward and I.M. George, "Dissolution of UO_2 in Molten Zircaloy-4, Part 1: Solubility from 2000 to 2200°C," *J. Nucl. Mater.* 208 (1994) 35.
 12. J. Rest and A.W. Cronenberg, "Modelling the Behavior of Xe, I, Cs, Te, Ba, and Sr in Solid and Liquefied Fuel During Severe Accidents," *J. Nucl. Mater.* 150 (1987) 203.
 13. L. Vath, "Modeling Transient Fission Gas Behavior for Solid, Melting and Molten Fuel in the Computer Program LAKU," *Nucl. Technol.* 98 (1992) 44.
 14. J. Crank, "The Mathematics of Diffusion," 2nd ed., p. 4, Oxford University Press, London (1975).
 15. D.S. Cox, F.C. Iglesias, C.E.L. Hunt, N.A. Keller, R.D. Barrand, J.R. Mitchell and R.F. O'Connor, "Oxidation of UO_2 in Air and Steam with Relevance to Fission Product Releases," *Proc. Symp. Chemical Phenomenon Associated with Radioactivity During Severe Nuclear Plant Accidents*, Anaheim, California, 9-12 September 1986, NUREG/CP-0078, p. 2, U.S. Nuclear Regulatory Commission (1986).
 16. J.A. Turnbull, C.A. Friskney, J.R. Findlay, F.A. Johnson and A.J. Walter, "The Diffusion Coefficients of Gaseous and Volatile Species During the Irradiation of Uranium Dioxide," *J. Nucl. Mater.* 107 (1982) 168.
 17. R.E. Carter and K.W. Lay, "Surface-Controlled Oxidation-Reduction of UO_2 ," *J. Nucl. Mater.* 36 (1970) 77.
 18. J.A. Meachen, "Oxygen Diffusion in Uranium Dioxide: A Review," *Nucl. Energy* 28 (1989) 221.

19. D.S. Cox, F.C. Iglesias, C.E.L. Hunt, R.F. O'Connor and R.D. Barrand, "High-Temperature Oxidation Behaviour of UO_2 in Air and Steam," Proc. Int. Symp. High-Temperature Oxidation and Sulphidation Processes, Hamilton, Ontario, Canada, August 26-30, 1990.
20. J. Abrefah, A. de Aguiar Braid, W. Wang, Y. Khalil and D.R. Olander, "High Temperature Oxidation of UO_2 in Steam-Hydrogen Mixtures," J. Nucl. Mater. 208 (1994) 98.
21. M.F. Osborne, J.L. Collins, R.A. Lorenz, J.R. Travis, C.S. Webster and T. Yamashita, "Data Summary Report for Fission Product Release Test VI-1," NUREG/CR-5339 (ORNL/TM-11104), Oak Ridge National Laboratory, June 1989.
22. M.F. Osborne, J.L. Collins, R.A. Lorenz, J.R. Travis and C.S. Webster, "Data Summary Report for Fission Product Release Test VI-2," NUREG/CR-5340 (ORNL/TM-11105), Oak Ridge National Laboratory, September 1989.
23. M.F. Osborne, R.A. Lorenz, J.L. Collins, J.R. Travis, C.S. Webster, H.K. Lee, T. Nakamura and Y.C. Tong, "Data Summary Report for Fission Product Release Test VI-3," NUREG/CR-5480 (ORNL/TM-11399 R3), Oak Ridge National Laboratory, June 1990.
24. M.F. Osborne, R.A. Lorenz, J.L. Collins, J.R. Travis, C.S. Webster and T. Nakamura, "Data Summary Report for Fission Product Release Test VI-4," NUREG/CR-5481 (ORNL/TM-11400 R3), Oak Ridge National Laboratory, January 1991.
25. M.F. Osborne, R.A. Lorenz, J.R. Travis, C.S. Webster and J.L. Collins, "Data Summary Report for Fission Product Release Test VI-5," NUREG/CR-5668 (ORNL/TM-11743), Oak Ridge National Laboratory, October 1991.
26. M.F. Osborne, R.A. Lorenz, J.R. Travis, C.S. Webster and J.L. Collins, "Data Summary Report for Fission Product Release Test VI-6," NUREG/CR-6077, Oak Ridge National Laboratory, unpublished report.
27. M.F. Osborne, R.A. Lorenz and J.R. Travis, "Preliminary Results from ORNL Fission Product Release Test VI-7," ORNL/NRC/LTR-94/2, Oak Ridge National Laboratory, February 1994.
28. M.F. Osborne, R.A. Lorenz, J.L. Collins and T. Nakamura, "Time-Dependent Release of Fission Products from LWR Fuel Under Severe Accident Conditions," Proc. Int. Conf. Thermal Reactor Safety, Avignon, France, October 2-7, 1988, p. 1293.
29. B. André, G. Ducros, J.P. Lévêque, D. Maro, M.F. Osborne and R.A. Lorenz, "Fission Product Releases at Severe LWR Accident Conditions: ORNL/CEA Measurements Versus Calculations," Commissariat à l'Énergie Atomique, unpublished report.
30. P.E. Blackburn, "Oxygen Pressures over Fast Breeder Reactor Fuel, (I) A Model for UO_{2+x} ," J. Nucl. Mater. 46 (1973) 244.
31. T.B. Lindemer and T.M. Besmann, "Chemical Thermodynamic Representation of $\langle UO_{2+x} \rangle$," J. Nucl. Mater. 130 (1985) 473.
32. H. Kleykamp, "The Chemical State of the Fission Products in Oxide Fuels," J. Nucl. Mater. 131 (1985) 221.

33. T. Yamashita, "Steam Oxidation of Zircaloy Cladding in the ORNL Fission Product Release Tests," ORNL/TM-10272, NUREG/CR-4777, Oak Ridge National Laboratory, March 1988.
34. B.J. Lewis and H.W. Bonin, "Transport of Volatile Fission Products in the Fuel-to-Sheath Gap of Defective Fuel Elements During Normal and Reactor Accident Conditions," J. Nucl. Mater. 218 (1994) 42.
35. B. André and G. Ducros, "The HEVA-VERCORS Program: Experimental Measurement of Fission Product Release Kinetics at Severe PWR Accident Conditions," Third Meeting of the European Severe Accident Chemistry Group JRC Karlsruhe, June 16-17, 1992.
36. J.P. Leveque, G. Lhiaubet and D. Boulaud, "HEVA Experimental Programme - Final Report," Technical Note DTP/SECC No. 69/91, Commissariat à l'Energie Atomique, November 1991.
37. J.K. Fink, M.G. Chasanov and L. Leibowitz, "Thermophysical Properties of Uranium Dioxide," J. Nucl. Mater. 102 (1981) 17.
38. R.E. Woodley, "The Viscosity of Molten Uranium Dioxide," J. Nucl. Mater. 50 (1974) 103.
39. CRC Handbook of Chemistry and Physics, 72nd Edition, CRC Press, Ann Arbor, 1991.
40. D.C. Douglas, "Atomic Energy Review, The Metallurgy of Zirconium," Supplement 1971, International Atomic Energy Agency, 1971.
41. D.R. Olander, "Fundamental Aspects of Nuclear Reactor Fuel Elements," TID-26711-P1, Atomic Energy Commission, 1976.
42. R.B. Bird, W.E. Stewart and E.N. Lightfoot, "Transport Phenomena," John Wiley and Sons, Inc., New York, 1965, p. 514.
43. R.C. Reid and T.K. Sherwood, "The Properties of Gases and Liquids," McGraw-Hill, New York, 1966, p. 544.
44. U.S. Nuclear Regulatory Commission, "Technical Basis for Estimating Fission Product Behaviour During LWR Accidents," NUREG-0772, June 1981.
45. P.R. McClure, M.T. Leonard and A. Razani, "A Model for Fission Product Release from Liquid-Metal Pools: Development and Sensitivity Investigation," Nucl. Sci. Eng. 114 (1993) 102.
46. D.R. Olander, "Oxidation of UO_2 by High-Pressure Steam," Nucl. Technol. 74 (1986) 215.
47. V.J. Wheeler and I.G. Jones, "Thermodynamic and Composition Changes in UO_{2+x} ($x < 0.005$) at 1950 K," J. Nucl. Mater. 42 (1972) 117.
48. P. Pascal, "Nouveau Traité de Chimie Minerale," Tome I, p. 484, Masson Editors, Paris (1956).
49. B. Morel, N. Serose, S. Gamaury, Ph. Dehaut, "Cinetique d'Oxydation du Combustible par la Vapeur d'Eau; Influence du S/V," Commissariat à l'Energie Atomique, Report NT/DTP/SECC no. DR94-55, June 1994.

TABLE 1: SUMMARY OF VERTICAL IRRADIATION (VI SERIES) TESTS AT-ORNL

Parameter	Test Number						
	VI-1	VI-2	VI-3	VI-4	VI-5	VI-6	VI-7
Fuel specimen							
Fuel type	Oconee	BR3	BR3	BR3	BR3	BR3	Monticello
Rod identification	1D13 (08747)	1-1002	1-1002	1-1059	1-114	1-114	BND0304 (G5)
Enrichment (wt% ²³⁵ U)	-	5.76	5.76	8.26	5.76	5.76	2.87
Zircaloy-4 cladding							
Outer diameter (cm)	1.08	0.95	0.95	0.95	0.95	0.95	1.243
Fuel length (cm)	15.2	15.2	15.2	15.2	15.2	15.2	15.2
Fuel loading (g U ₂ O ₅)	109.18	82.0	81.1	78.22	80.8	81.5	126.0
Weight of Zircaloy (g)	31.18	21.3	21.2	21.07	21.22	21.54	44.2
Total specimen weight (g)	140.36	103.3	102.3	99.29	102.0	103.0	170.2
Irradiation Data							
Irradiation period	2/75-11/79	7/76-9/80	7/76-9/80	7/76-9/80	7/76-9/80	7/76-9/80	7/74-2/80
Bumpup (MWd/kg U)	40	44	42	47	42	42	40
Max. heat rating (W/cm)	-	-	251	270	222	222	-
Grain radius (μm)	4.6	6.0	6.0	6.0	6.0	6.0	-
In-pile Kr release (%)	0.7	2	10	10	2	2	2
Test conditions							
Test temperature (K)	2020, 2300 ^(a)	2300	2000, 2700 ^(d)	2440	2015, 2740 ^(d)	2310	2025, 2307 ^(d)
Time at temperature (min)	20, 20	60	20, 20	20	20, 20	60	20, 20
Atmosphere ^(b)	Steam	Steam	Steam	Hydrogen	Hydrogen	Hydrogen, steam ^(c)	Air (with saturated water)
Flow rate (l/min)	1.54	1.54	1.6	0.4	0.4	0.4, 1.0	1.0 ^(d)
Fractional release (%)							
¹³⁷ Cs	63	67	100	96	100	80	71
⁸⁵ Kr	57	>31	100	85	100	75	65
¹²⁹ I	37	>33	-	71	-	-	-
¹³³ Sb	33	68	99	6.4	18	64	52
¹⁵⁴ Eu	0	0	-0.01	19	57	14	-
¹⁰⁶ Ru	0	0	5.0	0	0	0	-
Reference							
	21	22	23	24	25	26	27

- (a) Some tests (VI-1, VI-3, VI-5 and VI-7) were conducted in two phases at two different temperatures.
- (b) At standard temperature and pressure.
- (c) Test VI-6 was heated to 2300 K in hydrogen (Phase A) and then switched to a steam atmosphere (Phase B and C). During Phase B and the first 17 min of Phase C, steam flow across fuel specimen was reduced by an unknown amount because of leakage.
- (d) During test period 2000 to 2300 K (saturated water at 50°C).

TABLE 2: SUMMARY OF HEVA AND VERCORS TESTS AT CEA

Parameter	HEVA 01	HEVA 02	HEVA 03	HEVA 04	HEVA 05	HEVA 06	HEVA 07	HEVA 08	VERCORS 01	VERCORS 02
Test description										
Test type	-Commissioning test	-Commissioning test	-FPR at 2070 K in H ₂ O and H ₂ with irradiated fuel	-FPR at 2270 K in H ₂ O and H ₂ with irradiated/re-irradiated fuel	-FPR at 2070 K in H ₂ O and H ₂ with irradiated/re-irradiated fuel	-FPR at 2370 K in H ₂ with irradiated/re-irradiated fuel	-Release of Ag, In, Cd at 2070 K in H ₂ O and H ₂ with unirradiated fuel	-FPR at 2070 K in H ₂ O and H ₂ with Ag, In, Cd and irradiated/re-irradiated fuel	-FPR at 2130 K in H ₂ O and H ₂ with irradiated/re-irradiated fuel	-FPR at 2150 K in H ₂ O and H ₂ with irradiated/re-irradiated fuel
Fission Product Release (FPR) at 1900K in H ₂ O with irradiated fuel	-	-	-Aerosol sizing at 1070 K	-Aerosol sizing at 870 K	-Aerosol sizing at 520 K	-Aerosol sizing at 520 K	-Aerosol sizing at 520 K	-Aerosol sizing at 520 K	-Aerosol sizing at 870 K	-Aerosol sizing at 870 K
Fuel specimen										
Fuel type	CAP/2	CAP/2	BR3	Festenberg 1/2	Festenberg 1/2	Festenberg 1/2	-	Festenberg 1/2	Festenberg	Bugey/3
Rod identification	4026 (FROEDJZ)	4026 (FROEDJZ)	-	CT12 (FDC 57)	CT12 (FDC 57)	CT12 (FDC 57)	-	CT12 (FDC 57)	CO9 (FEC 57)	CT19 (FEC 53)
Enrichment (wt% ²³⁵ U)	4.95	4.95	8.6	3.1	3.1	3.1	depleted	3.1	3.1	3.1
Clad Outer Diam. (mm)	-	-	9.48	9.50	9.50	9.50	-	9.50	9.50	9.50
Pellet Outer Diam. (mm)	8.1	8.1	8.03	8.19	8.19	8.19	8.2	8.19	8.19	8.19
Pellet length (mm)	12	12	11/18	13.96	13.96	13.96	-	13.96	13.96	13.96
Initial fuel/clad gap (μm)	-	-	83.5	85	85	85	-	85	85	85
Fissile length (mm)	-	-	-	46	46	46	45	46	44	44
Sample height (mm)	-	-	-	80	80	80	80	80	87	80
Irradiation Data										
Irradiation period	5/78-3/80	5/78-3/80	-	3 cycles to 6/81	3 cycles to 6/81	3 cycles to 6/81	-	3 cycles to 6/81	4 cycles to 01/83	3 cycles to 02/83
Bumpup (MWd/kg U)	19.4	19.4	27.7	36.7	36.7	36.7	-	36.7	42.9	38.3
Avg. heat rating (W/cm)	-	-	250	185	185	185	-	185	-	-
Cooling period (y)	3.25	3.75	8	5.5	6	6.75	-	7.75	7	7
Grain radius (μm)	-	-	7.5	7.5	7.5	7.5	-	7.5	4	7.5
Re-irradiation	No	No	No	Yes	Yes	Yes	-	Yes	Yes	Yes
Test conditions										
Test date	6/83	11/83	2/86	12/86	6/87	3/88	6/88	3/89	11/89	6/90
Temperature rise (K/s)	1	1	1	1	1	2	1	1	1	1
Test temp. plateau (K)	1900	2140	2070	2270	2070	2370	2070	2070	2130	2150
Time at temp. plateau (s)	900	900	1800	420	5760	1800	1800	600	1020	780
Flow rate (mg/s)	-	-	0.5	0.5	0.5	0.2	0.5	0.5	0.05	0.5
H ₂	0	0	37	30	25	0	25	25	2.5	2.5
H ₂ O	100	30	37	30	25	0	25	25	2.5	2.5
Insulator temperature (K)	No	No	1070	870	520	520	520	520	870	870
Ag/In/Cd	No	No	No	No	No	No	Yes	Yes	No	No
Fractional release (%)										
¹³⁷ Cs	-2	68	38	44	66	30	-	15	42	28
¹³¹ I	-	-	-	43	62	30	-	12	31	24
¹³³ Cs	-	-	-	-42	-65	15	-	-	-35	-22
¹³⁷ Ce	-	-	-	52	54	11	-	5 (detection limit)	4.6	19
¹³³ Sb	1	41	20	18	11	0 (¹³³ Sb)	-	15 (detection limit)	-3	-7
¹⁰⁶ Ru	-	-	-	21	55	-4	-	16 (detection limit)	-	17
¹³⁷ Eu	-	-15	-	-	-	-5	-	-	-	-
¹³⁷ Ce	-	9 (detection limit)	<3	-	-	0 (¹³⁷ Ce)	-	-	-	-
¹⁰⁶ Ru	-	5 (detection limit)	<1.5	-	-	0 (¹⁰⁶ Ru)	-	-	-	-
¹⁰⁶ Ba	-	-	-	5.6	-	27	-	6 (detection limit)	-1.4	8

TABLE 3: VALUES OF VARIOUS PARAMETERS USED IN THE PRESENT STUDY

Symbol	Explanation of Parameter	Value	Ref.
A. Values Assumed in Study			
ρ_z	$= \rho_{UO_2}$ ^(b)	$8.74 \times 10^3 \text{ kg/m}^3$	
μ_z ^(a)	$= \mu_{UO_2}$ ^(b)	$4.3 \times 10^{-3} \text{ Pa}\cdot\text{s}$	
γ_z ^(a)	$= \gamma_{Zr}$ and $\gamma_{U,m}$ ^(b)	1.5 N/m	
r_U	Radius of uranium particle	$2.1 \times 10^{-10} \text{ m}$	
B. Physical Parameters and Constants			
$\rho_{UO_2,m}$	Density of uranium dioxide on melting	$8.74 \times 10^3 \text{ kg/m}^3$	37,38
$\rho_{Zr,m}$	Density of zirconium on melting	$5.8 \times 10^3 \text{ kg/m}^3$	39
$\mu_{UO_2,m}$	Viscosity of uranium dioxide on melting	$4.3 \times 10^{-3} \text{ Pa}\cdot\text{s}$	37,38
$\gamma_{Zr,m}$	Surface tension of zirconium on melting	$1.40 \text{ to } 1.48 \text{ N/m}$	9,39,40
$\gamma_{U,m}$	Surface tension of uranium on melting	1.5 N/m	39
Ω	Atomic volume	$41 \times 10^{-30} \text{ m}^3/\text{U-atom}$	41
g	Acceleration of gravity	9.807 m/s^2	39
k_B	Boltzmann's constant	$1.381 \times 10^{-23} \text{ J/K}$	39
C. V1-4 Analysis			
<i>(i) Experimental Parameters</i>			
$F_D(\tau_D)$	Cs release fraction at time of dissolution	27%	
M_c	Volatile gas concentration in melt	$2.8 \times 10^{23} \text{ atom/m}^3$	
r_{bc}	Critical bubble radius ^(c)	$0.057 \text{ }\mu\text{m}$	
T	Average temperature during dissolution	2373 K	
T_i	Period of release during dissolution	$1.74 \times 10^3 \text{ s}$	
<i>(ii) Model Parameters (Fitted)</i>			
f	Volume fraction of fuel dissolved	3.7%	
k	Cs rate constant for release from dissolved fuel	$4.6 \times 10^{-7} \text{ s}^{-1}$	
ϵ	Fraction of gas in bubbles	13% [Eqs. (B-11) and (B-14)]	

(a). Units are incorrect in Ref. 12.

(b). See item B.

(c). Bubble radius when random motion equals bias motion (for model calculation in Eqs. (B-11) and (B-14)).

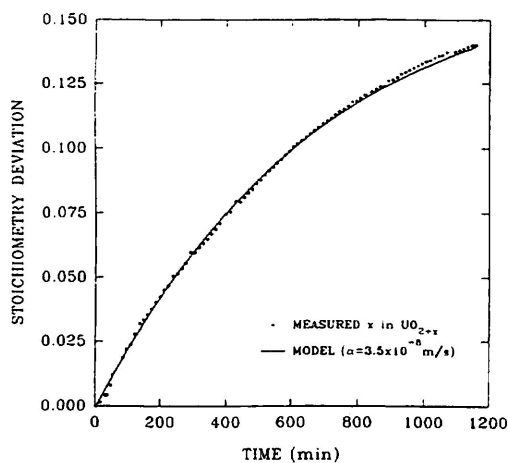


FIGURE 1. Oxidation kinetics of a sintered pellet ($S/V = 7 \text{ cm}^{-1}$) at 1473 K in He-3% H_2O (5 l/h) using a thermo-gravimetry technique at the CEA. The sample is taken to 1473 K under an inert atmosphere. At time zero, 3% H_2O is introduced into the carrier gas.

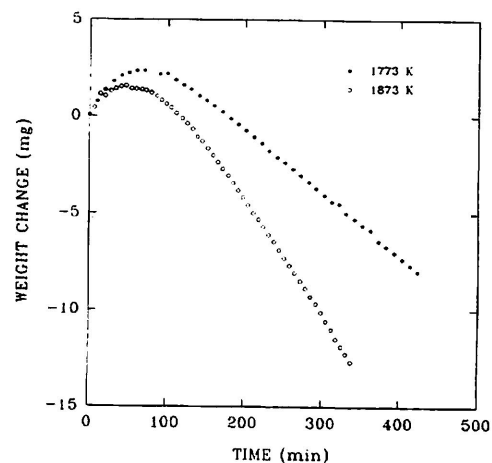


FIGURE 2. Weight evolution of sintered pellets ($S/V = 7 \text{ cm}^{-1}$) at 1773 K and 1873 K in He-1% H_2O (10 l/h). The initial weight of the sample is 0.7 g. The end-state stoichiometry deviation (after reduction in H_2) is determined to be 0.07 and 0.08 for the samples at 1773 and 1873 K, respectively.

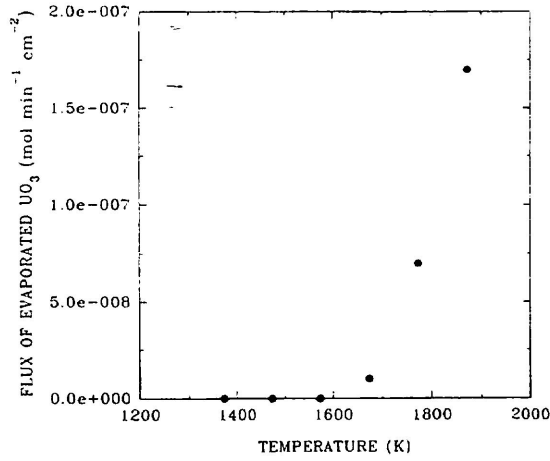


FIGURE 3. Fuel evaporation rate (in number of UO₃ mol per min per exposed pellet surface area) as a function of temperature.

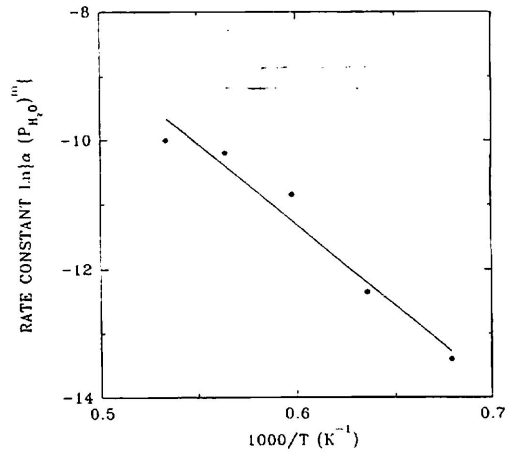


FIGURE 4. Plot of the quantity $\ln\{\alpha(P_{H_2O})^m\}$ as a function of temperature for the CEA experiments. The surface-exchange coefficient, α , is given in units of cm/s and the pressure, P_{H_2O} is given in units of atm.

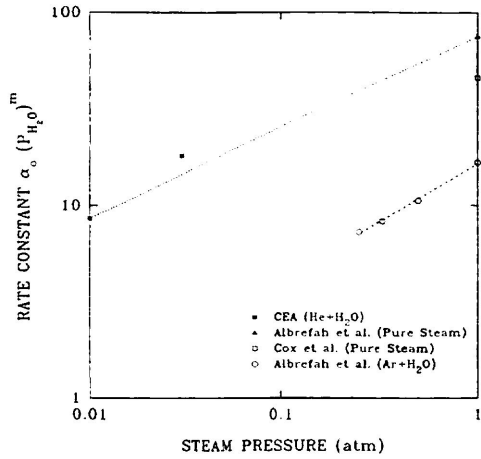


FIGURE 5. Plot of the quantity $\alpha_0(P_{H_2O})^m$ as a function of pressure for the CEA experiments. The quantity α_0 is given in units of cm/s and the pressure, P_{H_2O} is given in units of atm.

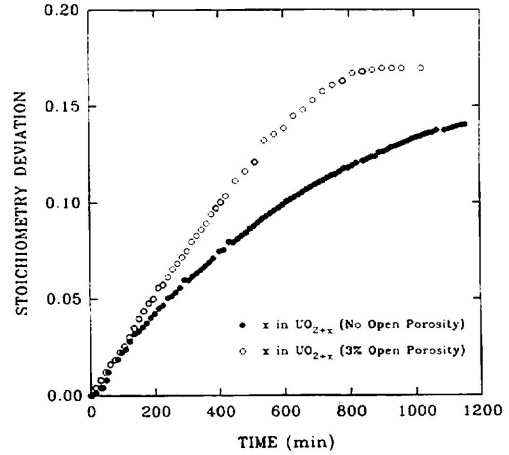


FIGURE 6. Comparison of fuel pellet oxidation with no open porosity and with 3% open porosity at 1473 K and in a He-3% H_2O (5 l/h) atmosphere.

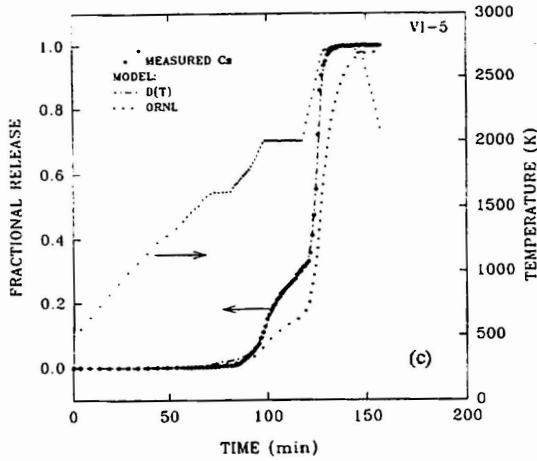
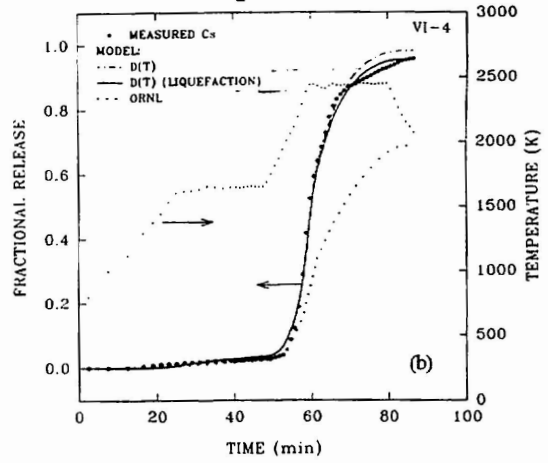
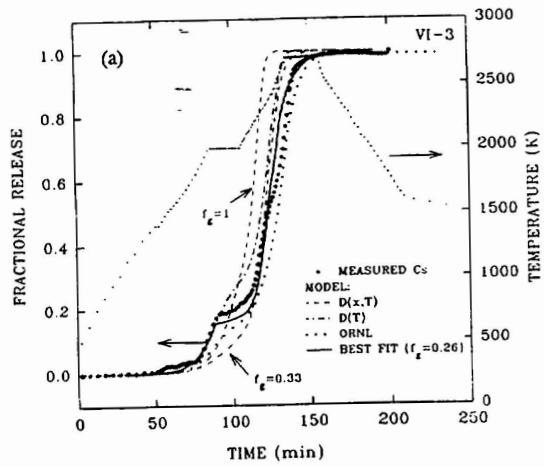


FIGURE 7. Measured and predicted release of cesium during the ORNL experiments conducted in a steam atmosphere: (a) VI-3, and in a hydrogen atmosphere: (b) VI-4 and (c) VI-5. The diffusion coefficients employed in the release models include: Eq. (11) for the ORNL model, Eq. (12) for the intrinsic diffusion model [labelled as D(T)], and Eqs. (5), (6) and (7) for the fuel oxidation/fission-product release model [labelled as D(x,T)]. The best-fit model uses the combined diffusion coefficient of Eq. (5) where the intrinsic diffusivity during the initial ramp is given by Eq. (12).

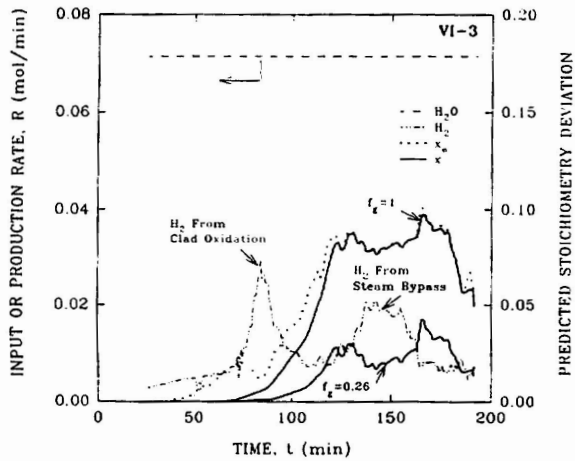


FIGURE 8. Steam input rate and hydrogen production rate for VI-3. The predicted equilibrium stoichiometry deviation (x_g) is given for $f_g = 1$. The stoichiometry deviation (x) is given for $f_g = 1$ and 0.26.

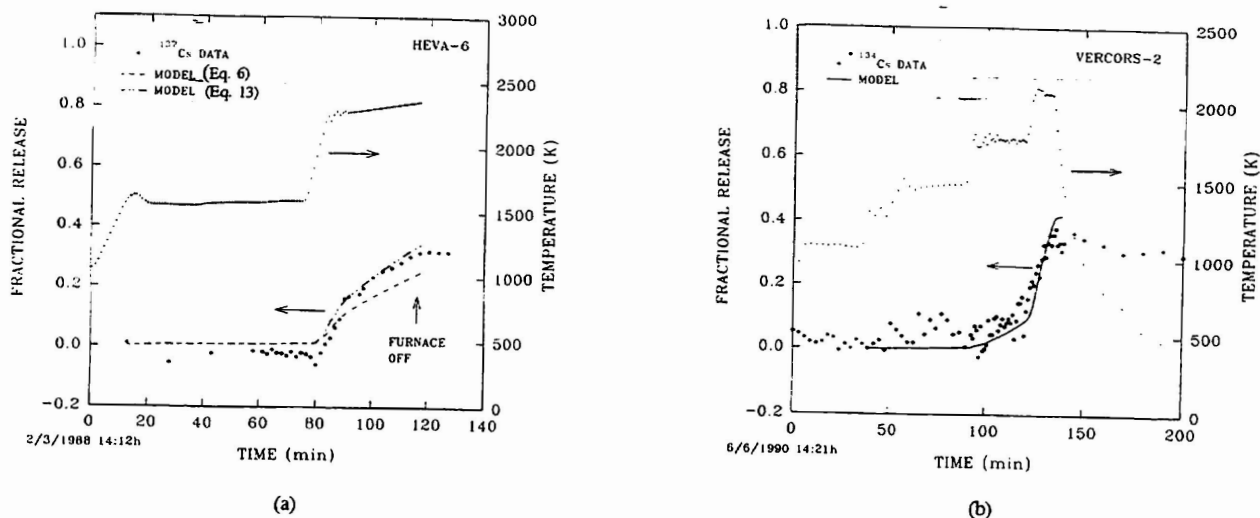


FIGURE 9. Comparison between measured and predicted fractional release values of cesium in CEA tests: (a) HEVA-6 and (b) VERCORS-2.

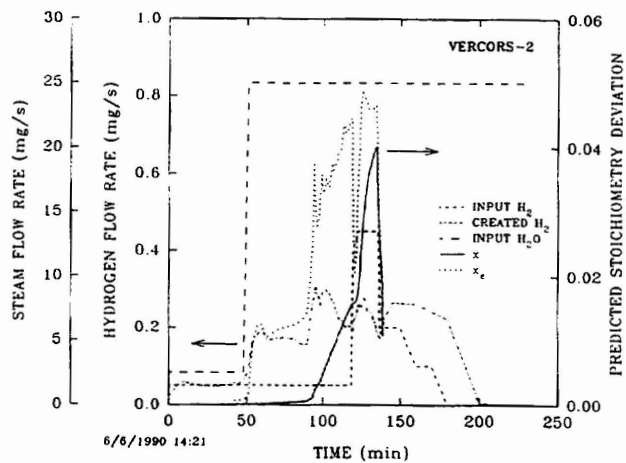


FIGURE 10. Steam and hydrogen input rates, and hydrogen production rate, for the VERCORS-2 test. The predicted equilibrium stoichiometry deviation (x_e) and stoichiometry deviation (x) are also given for $f_g = 0.174$.